Engineering a Cell-Surface Aptamer Circuit for Targeted and Amplified Photodynamic Cancer Therapy

Da Han,[†] Guizhi Zhu,[†,‡] Cuichen Wu,[†] Zhi Zhu,[‡,§] Tao Chen,[†] Xiaobing Zhang,[‡] and Weihong Tan[†,‡,*]

[†]Center for Research at Bio/Nano Interface, Department of Chemistry and Department of Physiology and Functional Genomics, Shands Cancer Center, UF Genetics Institute and McKnight Brain Institute, University of Florida, Gainesville, Florida 32611, United States, [‡]Molecular Science and Biomedicine Laboratory, State Key Laboratory of Chemo/Bio-Sensing and Chemometrics, College of Biology, College of Chemistry and Chemical Engineering, Collaborative Innovation Center for Chemistry and Molecular Medicine, Hunan University, Changsha 410082, China, and [§]State Key Laboratory of Physical Chemistry of Solid Surfaces, Key Laboratory of Chemical Biology of Fujian Province, Key Laboratory of Analytical Science, and Department of Chemical Biology, College of Chemistry and Chemical Engineering, Xiamen University, Xiamen 361005, China

ABSTRACT Photodynamic therapy is one of the most promising and noninvasive methods for clinical treatment of different malignant diseases. Here, we present a novel strategy of designing an aptamer-based DNA nanocircuit capable of selective recognition of cancer cells, controllable activation of photosensitizers, and amplification of photodynamic therapeutic effect. The aptamers can selectively recognize target cancer cells and bind to the specific proteins on cell membranes. Then the overhanging catalyst sequence on the aptamer can trigger a toehold-mediated catalytic strand displacement to activate the photosensitizer and achieve amplified therapeutic effect. The specific binding-induced activation allows the DNA circuit to distinguish diseased cells from healthy cells, reducing damage to nearby healthy cells. Moreover, the catalytic amplification reaction will only take place close to the target cancer cells, resulting in a high local concentration of singlet oxygen to selectively kill the target cells. The principle employed in this study demonstrated the feasibility of assembling a DNA circuit on cell membranes and could further broaden the utility of DNA circuits for applications in biology, biotechnology, and biomedicine.

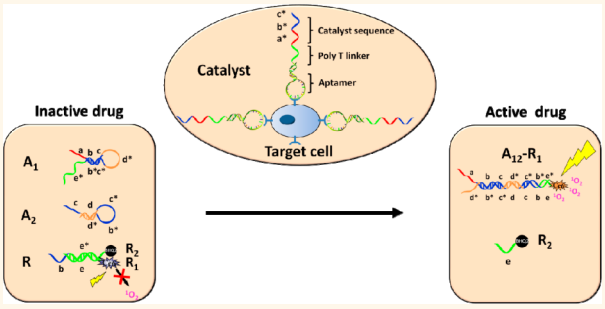

KEYWORDS: DNA nanocircuit · aptamer · photosensitizer · cancer therapy

As a minimally invasive therapeutic modality, photodynamic therapy (PDT) is already greatly used in clinical treatment of cancers. PDT can destroy cancer cells when light irradiates a photosensitizer (PS), generating reactive singlet oxygen ($^1O_2$).[1] Briefly, PDT involves a two-step process, whereby a nontoxic PS is delivered to an organism and then activated by an appropriate light source. However, because the $^1O_2$ has a limited lifetime and diffusion distance, efficient and reliable PDT depends on generating $^1O_2$ with methods that offer the greatest selectivity.[2]

PDT selectivity is usually controlled at two levels. The first level controls the spatial localization of PS reagents. This approach has been actively pursued by specifically delivering PS to the tumor site with regional light shining, which has effectively improved PDT selectivity and efficiency.[3,4] However, the tendency to cause damage to surrounding normal tissues still exists. To achieve greater selectivity, a molecular activation layer is added to further control the specificity of the PS. At this level, the probe initially stays in the nontoxic state and can only be activated when it interacts with its corresponding trigger at the tumor site. For example, we and others have developed activatable PDT methods which can be triggered by biomarkers, including membrane proteins[5] and extracellular proteases,[6] as well as cellular environments (*e.g.*, pH)[7] or other external stimuli, including artificial molecular switches.[8−10] Molecular activation allows the PS to distinguish diseased from healthy cells, thus greatly improving the selectivity of PDT.

To achieve higher oncolytic efficacy in tumors, a sufficient dosage of drugs should be administered at the tumor site. However, greater selectivity is typically achieved by

* Address correspondence to tan@chem.ufl.edu.

Received for review November 26, 2012 and accepted February 11, 2013.

Published online February 11, 2013
10.1021/nn305484p

introducing multiple activation processes but at the cost of decreasing the active drug amounts at the tumor site. For example, the triggers of activatable PDT are usually biomarkers present inside or outside the cells. However, the limited amount of trigger elements in the disease cells coupled with low activation efficiency may dramatically decrease the activation and killing effects of the PS. Selective amplification would effectively solve this problem. Researchers have applied some enzymes, such as protease whose overexpression is correlated with specific diseases, to continually catalyze PS activation, thereby amplifying the PDT effects.[11] However, the applications of enzymes are often limited by their microenvironment, including pH and temperature, in turn reducing the applications of enzyme-activatable PDT. Thus, to achieve more robust PDT with selectivity and amplification effect, a suitable medium is required that can both recognize the target cell and amplify the therapeutic effect.

As carriers of genetic information with well-regulated and predictable structures, nucleic acids are promising materials for signal amplification based on their nanometer size and programmability. Recent advances in the field of nucleic acids have generated nucleic-acid-based circuits, in which enzyme-free signal amplification can be achieved by simple nucleic acid hybridization, such as hybridization chain reaction,[12,13] entropy-triggered hybridization catalysis,[14] and DNA hairpin fuel catalysis.[15,16] These methods show promise in amplifying PDT with such properties as high amplification efficiency, environmental robustness, and ability to interact with other naturally occurring molecules. Meanwhile, the exploration and development of special single-stranded oligonucleotides, well-known as aptamers,[17−19] have extended the recognition capabilities of nucleic acids from Watson−Crick base pairing to interactions with various targets, such as small molecules,[20] proteins,[21] and cells,[22] *via* the aptamers' unique secondary or tertiary structures. We recently developed an effective method to generate aptamer-based molecular probes for the specific recognition and targeting of cancer cells.[22−25] Therefore, by combining the recognition and amplification abilities of these oligonucleotides, more efficient and specific PDT methods can be developed.

In this paper, we report the design of an aptamer-based DNA circuit capable of the selective recognition of cancer cells, controllable activation of PS, and amplification of therapeutic effect. In particular, the amplification circuit motif comprises two DNA hairpins developed by Yin *et al.*[15] and Li *et al.*[16] In principle, two DNA hairpin structures, $\mathbf{A_1}$ and $\mathbf{A_2}$, initially do not hybridize with each other because of the effective block created by complementary domains. However, in the presence of another ssDNA sequence, termed catalyst (**C**), $\mathbf{A_1}$ and $\mathbf{A_2}$ can form a stable duplex without consuming **C**. As shown in Figure 1, $\mathbf{A_1}$, $\mathbf{A_2}$, and **C** contain a few functional domains labeled in lowercase letters. Complementarity between lettered domains is denoted by an asterisk. Initially, **C** can hybridize with the exposed toehold domain **a** of $\mathbf{A_1}$ and gradually open the stem of $\mathbf{A_1}$ to form intermediate $\mathbf{A_1C}$, but $\mathbf{A_1C}$ has an exposed ssDNA domain **c*** able to hybridize with the exposed domain **c** in $\mathbf{A_2}$. Hence, after hybridization of **c** and **c***, the sequence **dc*b*d** will undergo branch migration and displace the **C** sequence (**c*b*a***) to form the $\mathbf{A_{12}}$ duplex. Importantly, the released **C** triggers further hybridizations of $\mathbf{A_1}$ and $\mathbf{A_2}$ in repeating cycles, thus providing the multiple-trigger effect absent in previous models. In this example, **C** catalyzes the formation of duplex $\mathbf{A_{12}}$ from $\mathbf{A_1}$ and $\mathbf{A_2}$ through a prescribed reaction pathway. The overall reaction is driven by a decrease in enthalpy, resulting from the formation of $\mathbf{A_{12}}$ with a greater number of base pairs.

Selectivity is achieved by encoding the catalyst sequence **C** (**a*b*c***) into an aptamer sequence (**Apt-C**) that targets cancer cells. To avoid forming undesired secondary structures, 17 poly-T bases are used to separate the aptamer sequence and **C**. Under these conditions, the aptamer part can bind to the receptor on the target cancer cell membrane with a tail (**C**) exposed for the catalytic hybridizations of $\mathbf{A_1}$ and $\mathbf{A_2}$. Thus, one aptamer binding event can induce multiple hybridization events between $\mathbf{A_1}$ and $\mathbf{A_2}$ to form dsDNA $\mathbf{A_{12}}$, and the all-important amplification step essentially derives from the catalytic reaction.

To apply this cell-catalyzed hairpin amplification circuit to PDT therapy, dsDNA sequences denoted as $\mathbf{R_{12}}$ are employed to carry the photodynamic therapeutic reagents. Because of its high photosensitizing efficacy and low dark toxicity, Chlorin e6 (Ce6), a second-generation and easily modifiable photosensitizer, is modified on ssDNA $\mathbf{R_1}$, and a quencher, BHQ2, is conjugated on ssDNA $\mathbf{R_2}$ to quench the generation of $^1O_2$ by Ce6 when no target cell is present. This design has several advantages. First, specific binding-induced activation allows the DNA circuit to distinguish diseased cells from healthy cells, reducing damage to nearby healthy cells which otherwise might be destroyed during PDT with conventional photosensitizers. Second, since the circulatory system *in vivo* can flush away the unbound aptamers and the catalyst **C** with aptamer is only present on the target cell membrane, the catalytic reaction will only take place close to the target cancer cells, resulting in a high local concentration of $^1O_2$ to selectively kill the target cells. Third, traditional aptamer-based PDT has suffered from the drawback of insufficient killing effects from the 1:1 binding-induced singlet oxygen generation (SOG). In this new design, by incorporating the catalyst sequences of the hairpin amplification circuit on cell membranes, numerous binding-induced SOG events can be realized on each cell membrane. In addition, the

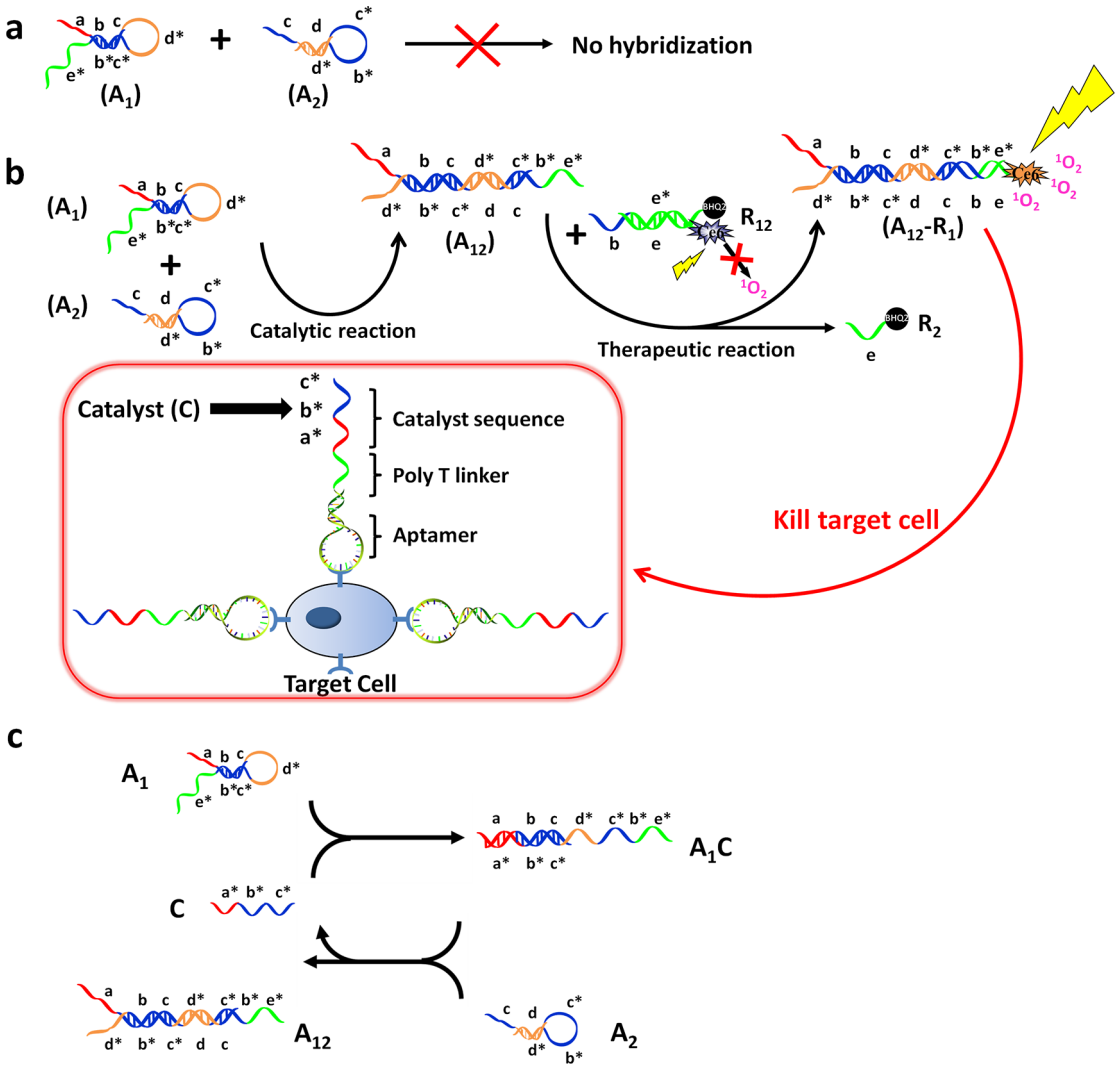

Figure 1. Working scheme of DNA aptamer circuit on cell membrane. (a) Scheme of the circuit without catalyst. (b) Scheme of the circuit on the cell membrane. The circuit involves two individual steps. In the catalytic step, the target cell labeled with Apt-C catalyzes DNA hairpins A_1 and A_2 to form duplex A_{12}. In the therapeutic step, A_{12} can open duplex R_{12} and displace quencher-labeled single-stranded R_2 to form A_{12}-R_1. Subsequently, Ce6-labeled R_1 generates singlet oxygen ($^1O_2$) to kill cancer cells by irradiation at 404 nm. (c) Scheme of detailed reaction of DNA hairpins A_1 and A_2 catalyzed by C sequence. Different domains are labeled with different colors. All x domains are complementary to x*.

uncatalyzed background of the circuit is nearly undetectable, resulting in fewer side effects to other healthy cells. Finally, to our best knowledge, this is the first design using the target cancer cell as the trigger to drive the DNA hybridizations. As such, this method may provide a universal strategy for signal amplification on cell membranes.

RESULTS AND DISCUSSION

To demonstrate the effectiveness of the **C** (**a*b*c***) in catalyzing the $\mathbf{A_1}$ and $\mathbf{A_2}$ hybridization, native gel electrophoresis was used. As shown in Figure S1 (Supporting Information), without **C**, $\mathbf{A_1}$ and $\mathbf{A_2}$ can be present stably without hybridization. However, when **C** is added, $\mathbf{A_1}$ and $\mathbf{A_2}$ hybridize with each other to form $\mathbf{A_{12}}$ with a yield even higher than that achieved by annealing of $\mathbf{A_1}$ and $\mathbf{A_2}$. To further study the amplification efficiency of the hairpin circuit, a FRET-based dsDNA $\mathbf{R_{12}}$ was designed with a stable fluorophore (FAM-$\mathbf{R_1}$) and quencher (DABCYL-$\mathbf{R_2}$) pair. To improve the thermostability and antienzymatic digestion ability of the $\mathbf{R_{12}}$ duplex, we incorporated 4 LNA (locked nucleic acid) nucleotides into FAM-labeled $\mathbf{R_1}$.[26] **C** was linked to an aptamer sequence TDO5, which targets acute lymphoblastic leukemia B-cells (K_d = 74.7 nM) *via* a poly-T linker.[23] Thus, **TDO5-C** was used as catalyst to initiate the $\mathbf{A_1}$/$\mathbf{A_2}$ hybridization, and the fluorescence was monitored. In the presence of different concentrations of **TDO5-C** (0−20 nM), dramatic signal enhancement was observed (Figure 2a), indicating the effective catalytic effect of **TDO5-C**. In addition, the signals approached a maximum in 2 h, indicating rapid kinetics of the catalytic hybridization.

We also studied the fluorescence kinetics of the 1:1 displacement reaction (Figure 2b). In particular, $\mathbf{A_{12}}$

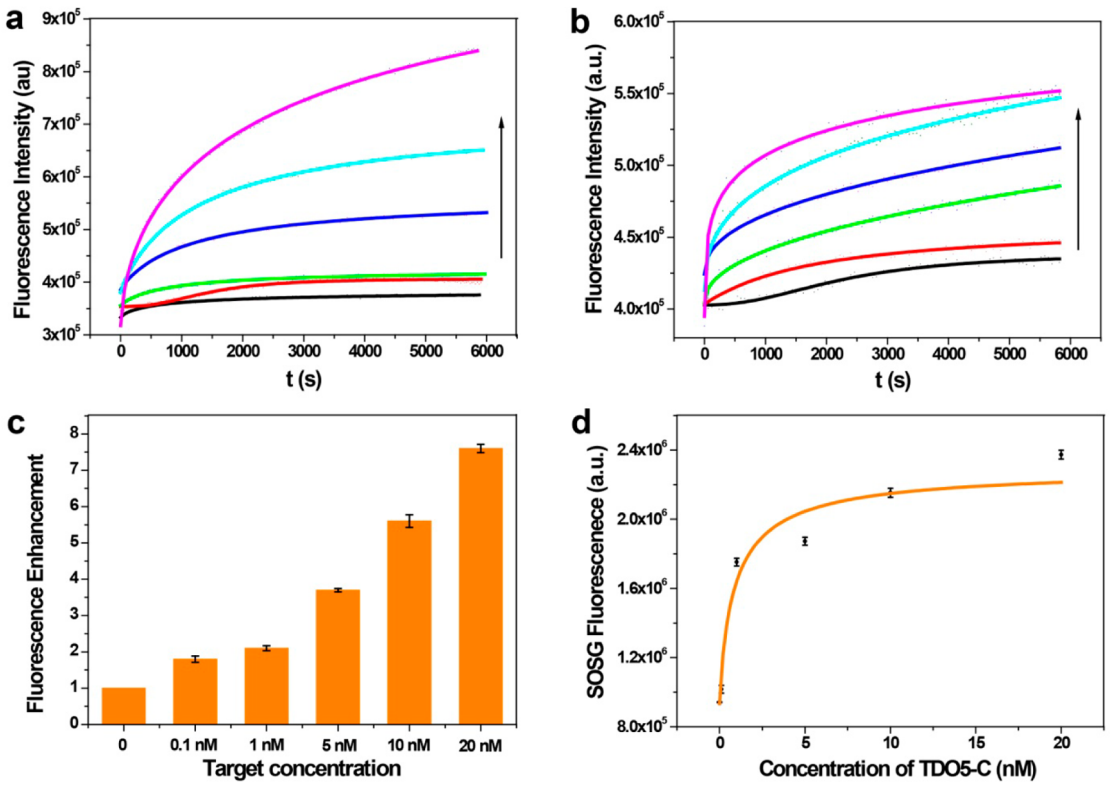

Figure 2. (a) Kinetics of DNA circuit containing A_1, A_2, and R_{12} with different concentrations of TDO5-C (fluorescence intensities corresponding to $F_{1:n}$) monitored by FAM fluorescence. The colored lines represent 0, 0.1, 1, 5, 10, and 20 nM of TDO5-C, respectively. (b) Kinetics of dsDNA R_{12} with different concentrations of A_{12} (fluorescence intensities corresponding to $F_{1:1}$) monitored by FAM fluorescence. The colored lines represent 0, 0.1, 1, 5, 10, and 20 nM of A_{12}, respectively. (c) Comparison of the fluorescence enhancement fold of the catalytic DNA circuit and 1:1 displacement. The calculation is based on the equation fold = $F_{1:n} - B/F_{1:1} - B$, where fold is the fluorescence enhancement ratio of 1:*n* method to 1:1 method and *B* is the background fluorescence. The fluorescence intensities at 6000 s are used to plot against different target concentrations. Each bar presents the mean and standard deviation derived from three independent experiments. (d) SOSG signal plotted as the function of TDO5-C concentration. The SOG was triggered by irradiation at 404 nm, the maximum absorption of Ce6, for 10 min. The SOSG fluorescence was obtained with excitation at 494 nm and emission from 500 to 600 nm. Each bar presents the mean and standard deviation derived from three independent experiments.

was prepared by annealing equal concentrations of **A_1** and **A_2** in advance. Then, different concentrations of **A_{12}** were added to displace **R_{12}** in buffer solution. In Figure 2c, the fluorescence enhancement ratio ($F_{1:n} - B/F_{1:1} - B$) between catalytic amplification circuit (1:*n*) and displacement reaction (1:1) is 8-fold at the target concentration of 20 nM after about 2 h, indicating high amplification efficiency of this circuit.

For therapeutic applications with the DNA circuit, **A_1**, **A_2**, and **R_{12}** will be present together in the deactivated forms around cells, and small leakage hybridizations may occur. Therefore, we tested the leakage hybridization rate by measuring the fluorescence of buffer solution containing **A_1**, **A_2**, and **R** without **TDO5-C** for 8 h (Figure S2). Although a small leakage did occur, the result indicated that the second-order rate constant of uncatalyzed reaction could be estimated to be $<10\ M^{-1}\ s^{-1}$, which is almost negligible for PDT applications.

Next, the photosensitizer Ce6 was conjugated to the ssDNA **R_1**, and the BHQ2 quencher was modified with ssDNA **R_2**. Because of the close proximity between Ce6 and BHQ2, up to 95% quenching efficiency of Ce6 was observed by our previous studies.[27] Herein, the DNA hairpin circuit had significant fluorescence enhancement upon the addition of different concentrations of **TDO5-C**. This was illustrated by the Ce6 fluorescence which increased up to 10-fold with 20 nM **TDO5-C** in buffer (Figure S3, Supporting Information). To evaluate the effect of different concentrations of **TDO5-C** on the amount of $^1O_2$ generated by Ce6-modified **R_1**, singlet oxygen sensor green (SOSG) was added, and its fluorescence enhancement was measured before and after irradiation at 404 nm. As shown in Figure 2d, SOSG fluorescence increased 3-fold with the introduction of 20 nM **TDO5-C** in the span of 1 h, indicating that SOG could be mediated by **TDO5-C**.

For proof of concept, a leukemia cell line was chosen as the target. Compared with solid tumor cells, leukemia cells are widespread in the circulatory system and are surrounded by normal blood cells. Under these circumstances, any nonspecific cytotoxin would also destroy the normal blood cells. Therefore, a therapeutic method which can selectively recognize and kill the target leukemia cells is highly desirable. As mentioned above,

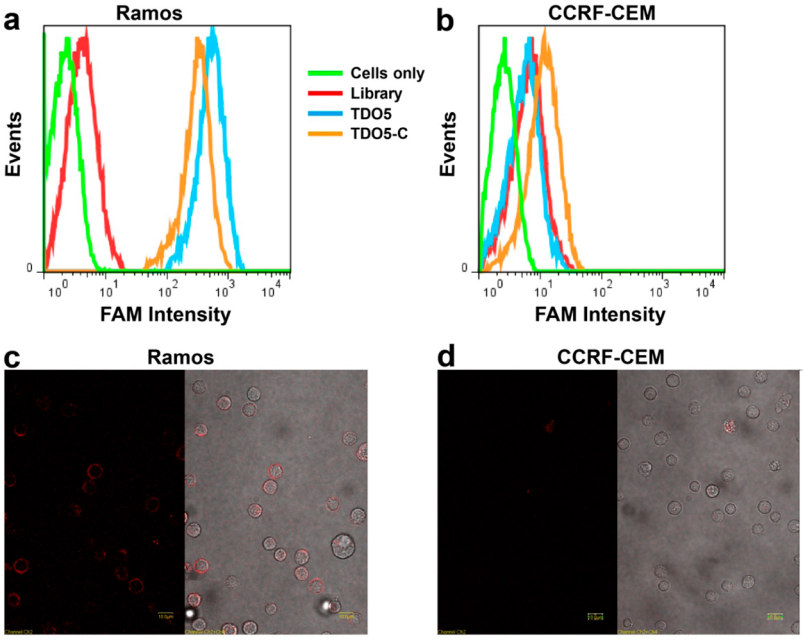

Figure 3. (a,b) Flow cytometry results of FAM-labeled TDO5-C binding with Ramos (a) and CCRF-CEM (b). Aptamer TDO5 was used as a positive control to show the maximum binding affinity. Cells: 200k/sample; aptamer concentration = 250 nM. (c,d) Confocal imaging of Ramos cells (c) and CCRF-CEM cells (d) incubated with 250 nM TMR-modified TDO5-C at 4 °C. Fluorescence image (left). Overlap of optical image and fluorescence image (right). The scale bar is 10 μm.

aptamer **TDO5**, which binds to the cancer cell membrane protein IgM with high affinity and selectivity, was used in our study with target cancer cell Ramos (acute lymphoblastic leukemia B-cells) and negative control cell CCRF-CEM (acute lymphoblastic leukemia T-cells). Therefore, if **TDO5-C** is present, it recognizes the target cancer cells and, importantly, also catalyzes the DNA hairpin hybridization to trigger SOG around cells. First, the selective binding of **TDO5-C** to Ramos cells was demonstrated by flow cytometry, as shown in Figure 3a, b. Herein, aptamer **TDO5** was used as a positive control. Compared with **TDO5**, **TDO5-C** showed almost equally strong binding affinity to Ramos cells at 4 °C, indicating that the cell membranes were partially covered by **TDO5-C**. However, both **TDO5** and **TDO5-C** exhibited weak affinity to the control CCRF-CEM cells, as evidenced by only small fluorescence peak shifts. In addition, to confirm that **TDO5-C** was bound to the cell membrane surface without internalization, confocal microscopy images were taken with TMR-labeled **TDO5-C** incubated with Ramos and CCRF-CEM cells (Figure 3c, d). Since only the cell membrane surface was labeled with fluorescence, the strong binding and low uptake efficiency of **TDO5-C** make it suitable for the catalysis of the hairpin circuit in close proximity to the target cancer cells.

To determine whether the amplification effect of **TDO5-C** remains active on the cell membrane, SOG was evaluated by incubating **TDO5-C**-labeled cells with the circuit ($\mathbf{A_1}$, $\mathbf{A_2}$, and $\mathbf{R_{12}}$) in PBS buffer, followed by adding SOSG sensor and monitoring the fluorescence. As shown in Figure 4, obvious SOSG fluorescence enhancement was observed when incubating the circuit with **TDO5-C**-labeled target cells (Ramos), which can be attributed to the catalytic effect of **TDO5-C** on the target cell membranes. As a control, the SOG triggered by **TDO5-C**-labeled CCRF-CEM cells was studied. Little SOSG fluorescence enhancement was observed compared to the circuit only ($\mathbf{A_1}$, $\mathbf{A_2}$, and $\mathbf{R_{12}}$), indicating that the selective binding of **TDO5-C** can induce selective SOG.

Cell destruction by PDT was studied by irradiation with white light. As indicated by the SOSG studies, $^1O_2$ is produced after the binding of **TDO5-C** with Ramos followed by the hybridization reaction of $\mathbf{A_1}$ and $\mathbf{A_2}$ to form $\mathbf{A_{12}}$ and the displacement of $\mathbf{R_1}$ from $\mathbf{R_{12}}$ by $\mathbf{A_{12}}$. Therefore, the phototoxicity of the cell-surface circuit to cancer cells was studied by MTS [3-(4,5-dimethylthiazol-2-yl)-5-(3-carboxymethoxyphenyl)-2-(4-sulfophenyl)-2*H*-tetrazolium] assay. After 3 h of light irradiation, the target cells (Ramos) and the control cells (CCRF-CEM) were cultured for 36 h before evaluating cell viability with MTS reagent. Figure 5 shows the MTS data expressed as the mean viability (standard deviation). The statistical differences were assessed by Student's *t* test. When $\mathbf{A_1}$, $\mathbf{A_2}$, and $\mathbf{R_{12}}$ were combined with nonlabeled cells and irradiated with white light, very little damage was observed to either target or control cells (cell viability of around 85%). These data are consistent with the previous SOG resulting from the weak leakage hybridizations of $\mathbf{A_1}$ and $\mathbf{A_2}$. However, when 100 nM free **C** was incubated with both cell lines, no statistical difference was evident ($P > 0.30$), and both cell types showed low cell viabilities of about

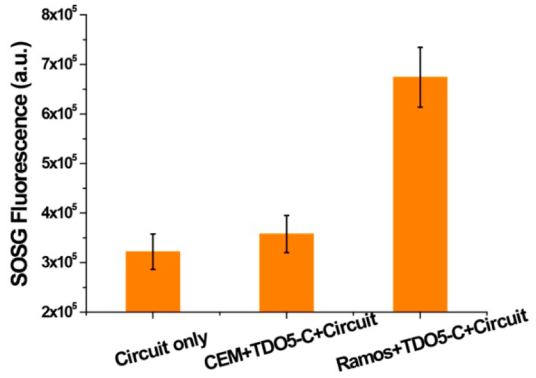

Figure 4. SOSG fluorescence of DNA circuit (A_1, A_2, and R_{12}) incubated with buffer, TDO5-C-labeled CCEF-CEM cells (control), and TDO5-C-labeled Ramos cells (target). Each bar presents the mean and standard deviation derived from three independent experiments (cells: 200k/sample; λ_{ex} = 494 nm and λ_{em} = 532 nm).

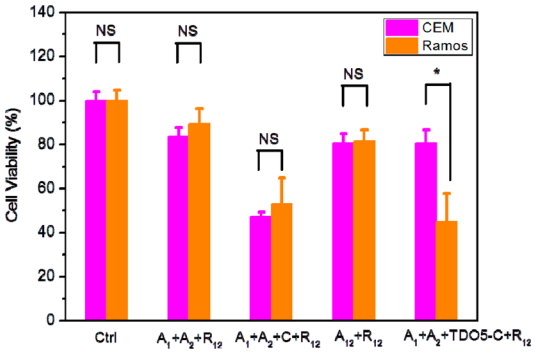

Figure 5. Cell viability result using MTS assay. The *in vitro* cytotoxicity was measured after 36 h of incubation in cell medium with 3 h of white light irradiation. Cells: 500k/sample. Each bar presents the mean and standard deviation derived from three independent experiments. *P* values were calculated by Student's test: ns, nonsignificance: $P > 0.30$ and * for $P < 0.02$, $n = 3$.

50%. Herein, because the free **C** sequence did not selectively recognize target cells, it catalyzed the amplification reaction without selectivity and caused relatively equal cell death for both target cells and control cells. On the other hand, when each of the cell lines was first incubated with **TDO5-C**, rinsed, and then incubated with $\mathbf{A_1}$, $\mathbf{A_2}$, and $\mathbf{R_{12}}$, high phototoxicity was observed for the target Ramos cells (45%), compared to 80% for the control cells (CCEF-CEM) with $P < 0.02$, indicating that **TDO5-C** can catalyze the hairpin circuit on specific cell membranes. In addition, we also found that the statistical toxicity difference between the ($\mathbf{A_1} + \mathbf{A_2} + \mathbf{C} + \mathbf{R_{12}}$) group and the ($\mathbf{A_1} + \mathbf{A_2} + \mathbf{TDO5\text{-}C} + \mathbf{R_{12}}$) group is evident ($P < 0.001$) for CEM cells but not for Ramos cells ($P > 0.3$) as the consequence of catalytic selectivity of **TDO5-C**. Finally, to compare the cytotoxicity of our method with the 1:1 displacement method, we incubated the preannealed $\mathbf{A_{12}}$ (1 μM) and $\mathbf{R_{12}}$ with cells and found a much higher cell viability of 79% for both cell lines. Under these conditions, the 1:1 displacement method did not show any selectivity to the two cell lines based on the lack of recognition element ($P > 0.30$). These comparisons demonstrate the selective and amplified therapeutic effect of our method.

CONCLUSION

In conclusion, our results demonstrate the feasibility of assembling a DNA circuit on cell membranes to achieve amplified and targeted photodynamic therapy. The DNA circuit, composed of four functional modules ($\mathbf{A_1}$, $\mathbf{A_2}$, $\mathbf{R_{12}}$, and **TDO5-C**) totally made of DNA, can greatly amplify the singlet oxygen generation and selectively kill cancer cells. In particular, the DNA hairpin amplification circuit can be catalyzed by specifically designed nucleic acid sequences. Many nucleic acids, including mRNA, microRNAs, and small interfering RNAs, are important biomarkers for various diseases.[28−30] If sequences for these biomolecules are available, the amplification hairpin DNA circuit can be designed to perform other biological and biomedical functions inside targeted disease cells with effective delivery methods. Second, increasing numbers of aptamers have been developed to target the membranes of a variety of cancer cell lines, thus establishing the universality of this DNA hairpin circuit for targeted and amplified therapy. Finally, as an application of DNA circuit to biological cells, the prototype DNA circuit demonstrated here has the potential to enhance DNA technology with new insights and will broaden the utility of DNA circuits for applications in biology, biotechnology, and biomedicine.

MATERIALS AND METHODS

Cell Culture. Ramos (CRL-1596, B-cell line, human Burkitt's lymphoma) and CCRF-CEM (CCL-119, T-cell line, human acute lymphoblastic leukemia) were cultured in RPMI 1640 medium (American Type Culture Collection) with 10% fetal bovine serum (FBS, Invitrogen, Carlsbad, CA, USA) and 0.5 mg/mL penicillin-streptomycin (American Type Culture Collection) at 37 °C under a 5% CO_2 atmosphere. Cells were washed before and after incubation with washing buffer [4.5 g/L glucose and 5 mM $MgCl_2$ in Dulbecco's PBS with calcium chloride and magnesium chloride (Sigma-Aldrich)]. Binding buffer used for selection was prepared by adding yeast tRNA (0.1 mg/mL; Sigma-Aldrich) and BSA (1 mg/mL; Fisher Scientific) to the wash buffer to reduce background binding.

Ce6-Modified DNA Synthesis. An amino group (Glen Research Corp.) was incorporated at the 5′-end using the synthesis protocol specified by the company. After removing the MMT protection group on the 5′-amino of the sequence on machine, the CPG beads were washed with acetonitrile (ACN) 10 times and dried with nitrogen for off-machine coupling of Ce6. Each Ce6 molecule has three carboxyl groups for conjugation with the amino group. To improve the coupling efficiency and reduce the multiple coupling products, the amount of Ce6 was 10 times more than DNA product in the coupling reaction. Ce6 (10 μmol) was mixed with an equal molecular amount of *N*,*N*′-dicyclohexylcarbodiimide (DCC, Sigma-Aldrich, Inc.) and *N*-hydroxysuccinimide (NHS, Sigma-Aldrich, Inc.) and dissolved in 250 μL of *N*,*N*-dimethylformamide (DMF) for the activation

reaction with 1 h stirring. The coupling reaction was performed with vigorous stirring overnight, followed by washing with ACN. Then the DNA product was purified by HPLC.

DNA Purification. Native PAGE was applied to purify the $\mathbf{A_1}$ and $\mathbf{A_2}$ hairpin strands to remove excess strands and avoid undesired system leakage. $\mathbf{A_1}$ and $\mathbf{A_2}$ were annealed at concentrations of around 50 μM in 1× TAE-Mg buffer (40 mM Tris-acetate-EDTA, pH 8.0, 12.5 mM $Mg(Ac)_2$) and cooled to room temperature. Native PAGE gels (12%) in 1× TAE-Mg buffer were run at 110 V for 90 min at 4 °C and stained with GelRed stain solution (Biotium, Inc., Hayward, CA). Only the sharp bands were cut from the gels, chopped into small pieces, and soaked in 1× TAE-Mg^{2+} buffer for 24 h. The buffer was extracted and concentrated with centrifugal filter devices (Millipore, Billerica, MA). Finally, the purified DNA sequences were quantified by UV spectrometry and kept in buffer for future use.

Fluorescence Kinetics of the DNA Hairpin Circuit in Buffer. All fluorescence measurements were performed using a Fluorolog (Jobin Yvon Horiba) with a 100 μL macrocuvette. DNA sequences $\mathbf{A_1}$ and $\mathbf{A_2}$ were separately refolded in the Fluo buffer (20 mM Tris, pH 7.5; 140 mM NaCl; 5 mM KCl). This and other refolding reactions involved heating to 90 °C for 1 min, followed by slowly decreasing the temperature to 25 °C at a rate of 0.1 °C s^{-1}. After purification by gel electrophoresis, the annealed sequences were stocked in Fluo buffer for later use. An amount of 10 μM stock of R was prepared by annealing 10 μM FAM-$\mathbf{R_1}$ and 15 μM DABCYL-$\mathbf{R_2}$ in Fluo buffer. An excess of $\mathbf{R_2}$ ensures efficient quenching of $\mathbf{R_1}$ but does not interfere with the readout of $\mathbf{A_1}$ and $\mathbf{A_2}$. A mixture of 100 nM $\mathbf{A_1}$, 100 nM $\mathbf{A_2}$, and 150 nM $\mathbf{R_{12}}$ was prepared in 1× Fluo buffer. The fluorescence at 518 nm was monitored at 25 °C after adding different amounts of **TDO5-C**. To evaluate the amplification effect of the circuit, a 1:1 displacement reaction was performed under the same conditions by mixing 10 μM $\mathbf{A_1}$ and $\mathbf{A_2}$ in 1× Fluo buffer and heating to 90 °C for 3 min, followed by slowly decreasing the temperature to 25 °C to form the stable duplex $\mathbf{A_{12}}$. A 150 nM sample of $\mathbf{R_{12}}$ was incubated in 1× Fluo buffer, followed by adding different concentrations of $\mathbf{A_{12}}$ and monitoring the fluorescence.

Test of the Fluorescence Response and SOG of the DNA Hairpin Circuit. For these experiments, Ce6-modifed $\mathbf{R_1}$ and BHQ2-modified $\mathbf{R_2}$ were used to form duplex $\mathbf{R_{12}}$. To study the Ce6 fluorescence response to different concentrations of **TDO5-C**, 100 nM $\mathbf{A_1}$, 100 nM $\mathbf{A_2}$, and 150 nM $\mathbf{R_{12}}$ were mixed in 1× Fluo buffer. The excitation wavelength was set at 404 nm with emission scanned from 600 to 800 nm. When testing the SOG, the concentration of the SOSG probe was set at 2 μM together with 100 nM $\mathbf{A_1}$, 100 nM $\mathbf{A_2}$, and 150 nM $\mathbf{R_{12}}$ in 1× Fluo buffer. To extend the lifetime of $^1O_2$ and increase the sensitivity of SOG assay, all buffers and samples were prepared using deuterium oxide. The SOG was triggered by irradiation at 404 nm, the maximum absorption of Ce6, for 10 min. The SOSG fluorescence was obtained with excitation at 494 nm and emission from 500 to 600 nm.

Test of the SOG Response of the DNA Hairpin Circuit to Cancer Cells. A quantity of 3×10^5 Ramos and CCRF-CEM cells was prepared in 100 μL of washing buffer separately. Fifty picomoles of nonlabeled **TDO5-C** was added and incubated for 30 min. After washing the cells twice with washing buffer, the two different cell types were resuspended in 100 μL of washing buffer. Then 100 nM $\mathbf{A_1}$, 100 nM $\mathbf{A_2}$, and 150 nM $\mathbf{R_{12}}$ were incubated with cells for 1 h. To extend the lifetime of $^1O_2$ and increase the sensitivity of the SOG assay, all buffers and samples were prepared using deuterium oxide. Two micromolar SOSG sensors were added to the cell medium, and SOG was triggered by irradiation at 404 nm, the maximum absorption of Ce6, for 10 min. The fluorescence was monitored at 25 °C with the excitation wavelength at 494 nm and emission from 500 to 600 nm.

Flow Cytometric Analysis. In flow cytometry tubes, 250 nM biotin-labeled **TDO5** or **TDO5-C** was incubated with 3×10^5 Ramos or CCRF-CEM cells at 4 °C in 200 μL of binding buffer for 30 min. The cells were washed twice with 1 mL of washing buffer, centrifuged at 1300 rpm for 3 min, and then resuspended in 200 μL of washing buffer. One microliter (1:400) of streptavidin-conjugated PE dye was incubated with the cells for another 20 min and washed twice using washing buffer. The cells were analyzed on a FACScan flow cytometer by counting 30 000 events. The PE-labeled unselected ssDNA library was used as a negative control.

Confocal Imaging of Cells Bound with Aptamer. For confocal imaging, the Ramos and CCEF-CEM cells were incubated with 50 pmol of TAMRA-labeled **TDO5-C** in 100 μL of binding buffer containing 20% FBS on ice for 30 min. The cells were washed twice with 1 mL of washing buffer, centrifuged at 1300 rpm for 3 min, and then resuspended in 100 μL of washing buffer. Twenty microliters of cell suspension bound with TAMRA-labeled **TDO5-C** was dropped on a thin glass slide placed above a 60× objective on the confocal microscope. Imaging of the cells was performed on an Olympus FV500-IX81 confocal microscope. A 5 mW, 543 nm He−Ne laser was the excitation source for TAMRA throughout the experiments. The objective used for imaging was a PLAPO60XO3PH 60× oil-immersion objective with a numerical aperture of 1.40 (Olympus).

Cytotoxicity Study. The cytotoxicity study was performed using the CellTiter 96 Aqueous One Solution cell proliferation assay (MTS) for Ramos and CCRF-CEM cell lines in a 96-well cell culture plate at 500k/well, 100 μL. Five groups of cell samples were set up as follows: group 1, cells only; group 2, cells + 3.3 μL of 30 μM $\mathbf{A_1}$, 1.3 μL of 77 μM $\mathbf{A_2}$, and 2 μL of 50 μM Ce6-modified $\mathbf{R_{12}}$; group 3, cells incubated with the same amount of $\mathbf{A_1}$, $\mathbf{A_2}$, and $\mathbf{R_{12}}$, together with 1 μL of 10 μM free **C**; group 4, cells incubated with 1 μL of 100 μM preannealed $\mathbf{A_{12}}$ and 2 μL of 50 μM Ce6-modified $\mathbf{R_{12}}$. For group 5, the cells were incubated with **TDO5-C** conjugates for 30 min at 4 °C, followed by centrifugation at 1300 rpm for 3 min to remove the unbound DNA. Then probes in the same amount as that of group 2 were added. All groups of cells were suspended in cell medium (no FBS) and then irradiated with white light on ice for 3 h. After irradiation, the cells were incubated in a CO_2 incubator for 36 h. Finally, a 6×-concentrated MTS solution (120 μL/well) in RPMI 1640 medium solution was added to each well and incubated at 37 °C for 2 h. The absorbance value at 490 nm was determined by a VersaMax microplate reader (Molecular Devices, Inc., Sunnyvale, CA).

Conflict of Interest: The authors declare no competing financial interest.

Acknowledgment. We thank Dr. K. R. Williams for manuscript review. This work is supported by grants awarded by the National Key Scientific Program of China (2011CB911000), the Foundation for Innovative Research Groups of NSFC (Grant 21221003), China National Instrumentation Program 2011YQ03012412, and by the National Institutes of Health (GM066137, GM079359, and CA133086).

Supporting Information Available: Materials and methods, DNA sequences, gel electrophoresis to demonstrate the catalysis effect of DNA circuit, and fluorescence measurement for the performance of the circuit. This material is available free of charge *via* the Internet at http://pubs.acs.org.

REFERENCES AND NOTES

1. Dougherty, T. J.; Gomer, C. J.; Henderson, B. W.; Jori, G.; Kessel, D.; Korbelik, M.; Moan, J.; Peng, Q. Photodynamic Therapy. *J. Natl. Cancer Inst.* **1998**, *90*, 889–905.
2. Bugaj, A. M. Targeted Photodynamic Therapy—A Promising Strategy of Tumor Treatment. *Photochem. Photobiol. Sci.* **2011**, *10*, 1097–1109.
3. Mallikaratchy, P.; Tang, Z.; Tan, W. Cell Specific Aptamer-Photosensitizer Conjugates as a Molecular Tool in Photodynamic Therapy. *ChemMedChem* **2008**, *3*, 425–428.
4. Yang, X.; Huang, J.; Wang, K.; Li, W.; Cui, L.; Li, X. Angiogenin-Mediated Photosensitizer-Aptamer Conjugate for Photodynamic Therapy. *ChemMedChem* **2011**, *6*, 1778–1780.
5. Wang, J.; Zhu, G.; You, M.; Song, E.; Shukoor, M. I.; Zhang, K.; Altman, M. B.; Chen, Y.; Zhu, Z.; Huang, C. Z.; *et al.* Assembly of Aptamer Switch Probes and Photosensitizer on Gold Nanorods for Targeted Photothermal and Photodynamic Cancer Therapy. *ACS Nano* **2012**, *6*, 5070–5077.
6. Zheng, G.; Chen, J.; Stefflova, K.; Jarvi, M.; Li, H.; Wilson, B. C. Photodynamic Molecular Beacon as an Activatable Photosensitizer Based on Protease-Controlled Singlet Oxygen Quenching and Activation. *Proc. Natl. Acad. Sci. U.S.A.* **2007**, *104*, 8989–8994.

7. McDonnell, S. O.; Hall, M. J.; Allen, L. T.; Byrne, A.; Gallagher, W. M.; O'Shea, D. F. Supramolecular Photonic Therapeutic Agents. *J. Am. Chem. Soc.* **2005**, *127*, 16360–16361.
8. Tang, Z.; Zhu, Z.; Mallikaratchy, P.; Yang, R.; Sefah, K.; Tan, W. Aptamer-Target Binding Triggered Molecular Mediation of Singlet Oxygen Generation. *Chem. Asian J.* **2010**, *5*, 783–786.
9. Zhu, Z.; Tang, Z.; Phillips, J. A.; Yang, R.; Wang, H.; Tan, W. Regulation of Singlet Oxygen Generation Using Single-Walled Carbon Nanotubes. *J. Am. Chem. Soc.* **2008**, *130*, 10856–10857.
10. Clo, E.; Snyder, J. W.; Voigt, N. V.; Ogilby, P. R.; Gothelf, K. V. DNA-Programmed Control of Photosensitized Singlet Oxygen Production. *J. Am. Chem. Soc.* **2006**, *128*, 4200–4201.
11. Chen, J.; Stefflova, K.; Niedre, M. J.; Wilson, B. C.; Chance, B.; Glickson, J. D.; Zheng, G. Protease-Triggered Photosensitizing Beacon Based on Singlet Oxygen Quenching and Activation. *J. Am. Chem. Soc.* **2004**, *126*, 11450–11451.
12. Dirks, R. M.; Pierce, N. A. Triggered Amplification by Hybridization Chain Reaction. *Proc. Natl. Acad. Sci. U.S.A.* **2004**, *101*, 15275–15278.
13. Huang, J.; Wu, Y.; Chen, Y.; Zhu, Z.; Yang, X.; Yang, C. J.; Wang, K.; Tan, W. Pyrene-Excimer Probes Based on the Hybridization Chain Reaction for the Detection of Nucleic Acids in Complex Biological Fluids. *Angew. Chem., Int. Ed.* **2011**, *50*, 401–404.
14. Zhang, D. Y.; Turberfield, A. J.; Yurke, B.; Winfree, E. Engineering Entropy-Driven Reactions and Networks Catalyzed by DNA. *Science* **2007**, *318*, 1121–1125.
15. Yin, P.; Choi, H. M. T.; Calvert, C. R.; Pierce, N. A. Programming Biomolecular Self-Assembly Pathways. *Nature* **2008**, *451*, 318–324.
16. Li, B.; Ellington, A. D.; Chen, X. Rational, Modular Adaptation of Enzyme-Free DNA Circuits to Multiple Detection Methods. *Nucleic Acids Res.* **2011**, *39*, e110.
17. Ellington, A. D.; Szostak, J. W. *In Vitro* Selection of RNA Molecules That Bind Specific Ligands. *Nature* **1990**, *346*, 818–822.
18. Tuerk, C.; Gold, L. Systematic Evolution of Ligands by Exponential Enrichment: RNA Ligands to Bacteriophage T4 DNA Polymerase. *Science* **1990**, *249*, 505–510.
19. Robertson, D. L.; Joyce, G. F. Selection *in Vitro* of an RNA Enzyme That Specifically Cleaves Single-Stranded DNA. *Nature* **1990**, *344*, 467–468.
20. Huizenga, D. E.; Szostak, J. W. A DNA Aptamer That Binds Adenosine and ATP. *Biochemistry* **1995**, *34*, 656–665.
21. Bock, L. C.; Griffin, L. C.; Latham, J. A.; Vermaas, E. H.; Toole, J. J. Selection of Single-Stranded DNA Molecules That Bind and Inhibit Human Thrombin. *Nature* **1992**, *355*, 564–566.
22. Shangguan, D.; Li, Y.; Tang, Z.; Cao, Z. C.; Chen, H. W.; Mallikaratchy, P.; Sefah, K.; Yang, C. J.; Tan, W. Aptamers Evolved from Live Cells as Effective Molecular Probes for Cancer Study. *Proc. Natl. Acad. Sci. U.S.A.* **2006**, *103*, 11838–11843.
23. Tang, Z.; Shangguan, D.; Wang, K.; Shi, H.; Sefah, K.; Mallikratchy, P.; Chen, H. W.; Li, Y.; Tan, W. Selection of Aptamers for Molecular Recognition and Characterization of Cancer Cells. *Anal. Chem.* **2007**, *79*, 4900–4907.
24. Sefah, K.; Tang, Z. W.; Shangguan, D. H.; Chen, H.; Lopez-Colon, D.; Li, Y.; Parekh, P.; Martin, J.; Meng, L.; Phillips, J. A.; *et al.* Molecular Recognition of Acute Myeloid Leukemia Using Aptamers. *Leukemia* **2009**, *23*, 235–244.
25. Shangguan, D.; Meng, L.; Cao, Z. C.; Xiao, Z.; Fang, X.; Li, Y.; Cardona, D.; Witek, R. P.; Liu, C.; Tan, W. Identification of Liver Cancer-Specific Aptamers Using Whole Live Cells. *Anal. Chem.* **2008**, *80*, 721–728.
26. Wang, L.; Yang, C. J.; Medley, C. D.; Benner, S. A.; Tan, W. Locked Nucleic Acid Molecular Beacons. *J. Am. Chem. Soc.* **2005**, *127*, 15664–15665.
27. Tang, Z.; Mallikaratchy, P.; Yang, R.; Kim, Y.; Zhu, Z.; Wang, H.; Tan, W. Aptamer Switch Probe Based on Intramolecular Displacement. *J. Am. Chem. Soc.* **2008**, *130*, 11268–11269.
28. Kim, V. N. Small RNAs: Classification, Biogenesis, and Function. *Mol. Cells* **2005**, *19*, 1–15.
29. Carthew, R. W.; Sontheimer, E. J. Origins and Mechanisms of miRNAs and siRNAs. *Cell* **2009**, *136*, 642–655.
30. Xie, Z.; Wroblewska, L.; Prochazka, L.; Weiss, R.; Benenson, Y. Multi-Input RNAi-Based Logic Circuit for Identification of Specific Cancer Cells. *Science* **2011**, *333*, 1307–1311.